International Journal of Heat and Mass Transfer 100 (2016) 332–346

Contents lists available at ScienceDirect

International Journal of Heat and Mass Transfer

journal homepage: www.elsevier.com/locate/ijhmt

A RANS model for heat transfer reduction in viscoelastic turbulent flow

M. Masoudian [a,*], F.T. Pinho [a], K. Kim [b], R. Sureshkumar [c,d]

[a] Transport Phenomena Research Center, Faculty of Engineering, University of Porto, Rua Dr. Roberto Frias s/n, 4200-465 Porto, Portugal
[b] Department of Mechanical Engineering, Hanbat National University, 125 Dongseo-daero, Yuseong-gu, Daejeon 305-701, South Korea
[c] Department of Biomedical and Chemical Engineering, Syracuse University, NY 13244, USA
[d] Department of Physics, Syracuse University, NY 13244, USA

ARTICLE INFO

Article history:
Received 8 September 2015
Received in revised form 12 April 2016
Accepted 18 April 2016

Keywords:
Newtonian and viscoelastic DNS
Drag reduction
FENE-P fluid
Viscoelastic RANS model
Heat transfer reduction

ABSTRACT

Direct numerical simulations (DNS) were carried out to investigate turbulent heat transfer in a channel flow of homogenous polymer solutions described by the Finitely Extensible Nonlinear Elastic-Peterlin (FENE-P) constitutive model at intermediate and high Prandtl numbers ($Pr = 1.25$ and 5). Time-averaged statistics of temperature fluctuations, turbulent heat fluxes, thermal turbulent diffusivity, and of budget terms of the temperature variance are reported and compared with those of the Newtonian fluid cases at the same Prandtl and Reynolds numbers. Moreover, twenty one sets of DNS data of fluid flow are utilized to improve existing k–ε–$\overline{v^2}$–f models for FENE-P fluids to deal with turbulent flow of dilute polymer solutions up to the high drag reduction regime; specifically the dependency of closures on the wall friction velocity is removed. Furthermore, five sets of recent DNS data of fluid flow and heat transfer of FENE-P fluids were used to develop the first RANS model capable of predicting the heat transfer rates in viscoelastic turbulent flows. In this model, an existing closure for calculating the turbulent Prandtl number for Newtonian fluids is extended to deal with heat transfer in turbulent viscoelastic fluids. Predicted polymer stresses, velocity profiles, mean temperature profiles, and turbulent flow characteristics are all in good agreement with the DNS data, and show improvement over previous RANS models.

1. Introduction

Drag reduction by addition of polymer molecules to the turbulent flow has been extensively investigated both experimentally and numerically over the last decades; comprehensive early reviews on the subject are those of Hoyt [1], Lumley [2] and Virk [3]. From the outset it was observed that the addition of small amounts of high molecular weight linear polymers, such as polyethylene oxide (PEO) or polyacrylamide among others, to low viscosity Newtonian solvents flowing in turbulent pipe or channel flow would reduce drag by up to 80%.

Recent comprehensive theories on the mechanisms of drag reduction induced by polymer additives have been put forward in the literature [4,5]. The mechanism is based on the fact that polymer molecules undergo a coil-to-stretch transition, causing an increase in the extensional viscosity of the solution that helps suppress Reynolds stress-producing events.

Over the last two decades, the development of accurate and efficient numerical and experimental methods for viscoelastic fluids has made it possible to investigate in detail turbulent DR in dilute polymer solutions [6–12]. Most of the numerical simulations used constitutive equations based on the FENE-P (Finitely Extensible Nonlinear Elastic with Peterlin closure) rheological constitutive equation which allows one to probe the effects on the flow of the polymer relaxation time, chain extensibility and of the ratio of polymer to solution viscosities. In this constitutive equation, a polymer chain is represented by a single dumbbell consisting of two beads, representing the hydrodynamic resistance, connected by a finitely extensible entropic spring.

Direct numerical simulations (DNS) of polymer induced drag reduction in turbulent channel flows up to the maximum drag reduction (MDR) limit were carried out using a fully spectral method by Ptasinski et al. [7], Dubief et al. [8], Dimitropoulos et al. [9], Thais et al. [10,11] and Li et al. [12]. They showed that to obtain significant levels of drag reduction large polymer chain extensibilities and high Weissenberg numbers are required. In addition, they studied the influence of rheological parameters of the FENE-P model on the amount of polymer-induced drag reduction.

* Corresponding author.
E-mail addresses: mmasoudian@fe.up.pt (M. Masoudian), fpinho@fe.up.pt (F.T. Pinho), kkim@hanbat.ac.kr (K. Kim), rsureshk@syr.edu (R. Sureshkumar).

http://dx.doi.org/10.1016/j.ijheatmasstransfer.2016.04.053
0017-9310/

Nomenclature

Symbol	Description
C	Conformation tensor
C_p	Specific heat capacity
Ep	Viscoelastic contribution of dissipation equation
$f(C_{kk})$	Peterlin function ($f(c_{kk}) = (L^2 - 3)/(L^2 - c_{kk})$)
$f(L^2)$	Peterlin function for the polymer maximum length ($f(L^2) = 1$)
f	Redistribution function
h	Half width of the channel ($h = 1$)
H^*	Hookean dumbbell spring constant
κ	Isotropic artificial numerical diffusivity constant
k	Turbulent kinetic energy
K	Thermal conductivity
L_t	Turbulence length scale
L^2	Polymer maximum extension length
M	Mean flow distortion term of conformation tensor
S	Rate of strain tensor
P_k	Turbulence production
Pe_t	Turbulent Peclet number ($Pe_t = v_T Pr/v$)
Pr	Molecular Prandtl number
Pr_t	Turbulent Prandtl number
$Pr_{t,extended}$	Extended turbulent Prandtl number
q''	Wall heat flux
$Re_{\tau 0}$	Reynolds number based on friction velocity ($Re_{\tau 0} = hU_\tau/v_0$)
u_i	Velocity vector
T	Instantaneous temperature
T^*	Friction temperature
T_t	Turbulence time scale
$Wi_{\tau 0}$	Weissenberg number based on friction velocity ($Wi_{\tau 0} = \lambda U_\tau^2/v_0$)
U_τ	Friction velocity
x, y, z	Coordinates in streamwise, wall-normal and spanwise directions, respectively

Greek symbols

α_t	Turbulent thermal diffusivity ($\alpha_t = v_t/Pr_t$)
β	Ratio between the solvent viscosity and the viscosity of the solution
ε	Dissipation rate of turbulence
ε_p	Viscoelastic stress work
η_p	Polymer viscosity coefficient
η_s	Solvent viscosity coefficient
v_T	Turbulent viscosity
$v_{T,P}$	Viscoelastic turbulent viscosity
λ	Polymer relaxation time
θ^+	Normalized instantaneous temperature by friction temperature
Θ^+	Reynolds averaged temperature normalized by friction temperature
ρ	Density
δ_{ij}	Kronecker delta

List of abbreviations

DR	Drag reduction
HDR	High drag reduction
IDR	Intermediate drag reduction
LDR	Low drag reduction
NLT	Nonlinear term in time averaged conformation tensor

Passive scalar transport in turbulent channel flow of viscoelastic dilute polymer solutions has been much less studied using direct numerical simulations, but nevertheless an investigation for DR of up to 74% was carried out by Gupta et al. [13]. They showed that DR is accompanied by increased coherence of the low-speed streaks in the buffer layer and that they are responsible for the streamwise heat transport, which is actually enhanced relative to the corresponding flux for Newtonian flow. Simultaneously the wall-normal and spanwise heat fluxes decrease with DR very much as happens with the Reynolds shear stress and the root mean square fluctuations in the wall-normal and spanwise directions. The enhanced anisotropy of the scalar heat fluxes, and in particular the enhancement of the streamwise heat flux, are rather unexpected results, whereas the reduced flow-normal heat flux was somewhat expected.

Yu et al. [14] carried out DNS of fully developed turbulent heat transfer of a viscoelastic drag-reducing flow described by Giesekus model at low Prandtl number ($Pr = 0.71$) and reported turbulent thermal statistics such as temperature fluctuations, turbulent heat fluxes and budget terms of the temperature variance and compared with those of a Newtonian fluid flow.

DNS simulation of turbulent viscoelastic flow is significantly more expensive than Newtonian DNS [12,15]. Hence, Reynolds-Averaged Navier–Stokes (RANS) [15–19], and Large Eddy Simulation (LES) models [21,22] have been developed over the years.

In the context of k–ε turbulence models for viscoelastic fluids Pinho et al. [16], and subsequently Resende et al. [17] proposed closures for Reynolds stresses of viscoelastic fluids described by the FENE-P model that relied on *a priori* analyses of DNS data. In these works Reynolds averaged flow and conformation quantities were predicted well, but both models were limited to applications in the low DR regime (DR < 34%). In addition both models rely on overly complex viscoelastic closures, they do not cover the whole range of drag reduction and do not deal easily with simulations in complex geometries, since they rely on the friction velocity instead of relying exclusively on local quantities for generality.

More recently Takahiro et al. [18] proposed a low Reynolds number k–ε model for viscoelastic fluids described by the Giesekus constitutive equation. Their closure is valid up to the maximum DR. In their proposal, an extra damping function was added to the closure of eddy viscosity, while the treatment of the turbulent kinetic energy (k) and its dissipation rate (ε) is an extension of their adopted base model for Newtonian fluids.

The first turbulence model of first order to be capable of predicting turbulent viscoelastic flows in the high drag reduction regime was developed by Iaccarino et al. [19] in the context of k–ε–$\overline{v^2}$–f model. Their model is based on a simplified representation of the polymer conformation tensor; in particular, they only consider the extension of the chains as characterized by the trace of the conformation tensor. They used the concept of turbulent polymer viscosity to account for the combined effects of turbulence and viscoelasticity on the momentum and conformation equations. Their closure for turbulent polymer viscosity depends on the turbulent kinetic energy, the polymer relaxation time and the trace of conformation tensor and the model of the nonlinear terms in the conformation tensor equation relied on the turbulent dissipation rate. However, although their model predicts accurately the amount of drag reduction, their predictions of the polymer shear stress, of the budget of the turbulent kinetic energy and of the various contributions to the evolution equation for the conformation tensor are not in agreement with DNS results.

Later, Masoudian et al. [15] using the *a priori* analyses of the DNS data proposed a new turbulence model for FENE-P fluids in the context of k–ε–$\overline{v^2}$–f, which was also valid up to the maximum amount of DR, and relying also on the concept of turbulent polymer viscosity previously introduced by Iaccarino et al. [19]. Relative to Iaccarino's model [19] they improved the predictions of the viscoelastic stress and of the viscoelastic stress work, which is the main viscoelastic contribution in the turbulent kinetic energy transport equation. Instead of using the turbulent dissipation rate to model the non-linear term in the conformation equation, as previously done by Iaccarino et al. [19], by analyzing DNS data Masoudian et al. [15] introduced a Boussinesq-like relation to model the non-linear contribution (*NLT*) in the conformation equation, and their model was validated over a wide range of rheological and flow parameters.

The single-point turbulence model developed here is based on the time-averaged governing equations for viscoelastic fluids presented originally by Masoudian et al. [15] and Iaccarino et al. [19]. An important contribution of the present work is the development of a single closure for the nonlinear fluctuating terms appearing in the FENE-P rheological constitutive equation by using a Boussinesq like relation to model the non-linear term (*NLT*). In addition, the dependency of the previously developed closure on the wall friction velocity is eliminated, i.e. all closures are now based on the local quantities, which give the model the capacity to be used in complex geometries. Furthermore, as far as we are aware of, there is no RANS model to deal with heat transfer in turbulent flows of viscoelastic fluids, so in this work the closure of Kays [20] is extended for the first time to cope with viscoelastic fluids. Five sets of recent DNS data for channel flow of viscoelastic fluids pertaining to low, intermediate and high drag reductions are used to quantify the heat transfer in viscoelastic turbulent flows.

The paper is organized as follows: Section 2 introduces the governing equations and identifies the viscoelastic terms requiring modeling, Section 3 introduces the numerical methods applied in DNS and reports time averaged statistics, in Section 4 the turbulent closures are developed and Section 5 presents model predictions. Conclusions are offered in Section 6.

2. Governing equations

In what follows, upper-case letters or overbars denote Reynolds-averaged quantities and lower-case letters or primes denote fluctuating quantities. Since the work makes significant improvements on an existing k–ε–$\overline{v^2}$–f model, prior to presenting the new closure for the Reynolds scalar fluxes the governing equations are presented first for isothermal flows and subsequently the thermal energy equation and the required closure are presented. Details on the Reynolds averaging procedure can be found elsewhere [15,19].

2.1. Momentum equation

The instantaneous momentum equation appropriate for the FENE-P fluids can be expressed as,

$$\rho\frac{\partial u_i}{\partial t}+\rho u_k\frac{\partial u_i}{\partial x_k}=-\frac{\partial p}{\partial x_i}+\frac{\partial \tau_{ik}}{\partial x_k} \tag{1}$$

where τ_{ik} is the fluid stress tensor, u_i is the velocity, p is the pressure, and ρ is the fluid density. The fluid extra stress tensor in Eq. (1) is given in Eq. (2) as the sum of a Newtonian solvent contribution of viscosity η_s with a polymeric contribution $\tau_{ij,p}$ described by the FENE-P rheological constitutive model.

$$\tau_{ij}=2\eta_s S_{ij}+\tau_{ij,p} \tag{2}$$

S_{ij} is the rate of strain tensor defined as

$$S_{ij}=\frac{1}{2}\left(\frac{\partial u_i}{\partial x_j}+\frac{\partial u_j}{\partial x_i}\right) \tag{3}$$

In the context of RANS, the instantaneous quantities are decomposed into mean and fluctuating components (Reynolds decomposition). Using this process in the momentum equation and subsequently averaging, the Reynolds averaged momentum equation is described by,

$$\rho\frac{\partial U_i}{\partial t}+\rho U_k\frac{\partial U_i}{\partial x_k}=-\frac{\partial \overline{P}}{\partial x_i}-\frac{\partial}{\partial x_k}\rho(\overline{u_i u_k})+\frac{\partial \overline{\tau}_{ik}}{\partial x_k} \tag{4}$$

where $\rho\overline{u_i u_k}$ is the Reynolds stress tensor. Note that overbars or uppercase letters denote Reynolds-averaged quantities.

2.2. Constitutive equation

In the FENE-P model the polymeric contribution to the total extra stress, Eq. (2), is given as an explicit function of the conformation tensor c_{ij}

$$\tau_{ij,p}=\frac{\eta_p}{\lambda}\left[f(c_{kk})c_{ij}-f(L)\delta_{ij}\right] \tag{5}$$

where λ is the polymer relaxation time, η_p is the zero shear rate polymer viscosity, and $f(c_{kk})$ is the Peterlin function, which takes here the form used by Li et al. [12] and given by,

$$f(c_{kk})=\frac{L^2-3}{L^2-c_{kk}}\ \text{together with}\ f(L)=1 \tag{6}$$

In this equation L^2 is the dimensionless polymer dumbbell maximum extension length.

In Eq. (5) the conformation tensor components must be calculated using the FENE-P evolution equation for c_{ij},

$$\frac{\partial c_{ij}}{\partial t}+u_k\frac{\partial c_{ij}}{\partial x_k}-\left(c_{jk}\frac{\partial u_i}{\partial x_k}+c_{ik}\frac{\partial u_j}{\partial x_k}\right)=-\frac{\tau_{ij,p}}{\eta_p} \tag{7}$$

By Reynolds averaging the instantaneous equations of the FENE-P model the following Reynolds-averaged conformation tensor equation is obtained,

$$U_k\frac{\partial C_{ij}}{\partial x_k}+\underbrace{\overline{u_k\frac{\partial c_{ij}}{\partial x_k}}}_{CT_{ij}}-\underbrace{\left(C_{jk}\frac{\partial U_i}{\partial x_k}+C_{ik}\frac{\partial U_j}{\partial x_k}\right)}_{M_{ij}}-\underbrace{\left(\overline{c_{jk}\frac{\partial u_i}{\partial x_k}}+\overline{c_{ik}\frac{\partial u_j}{\partial x_k}}\right)}_{NLT_{ij}}$$
$$=-\underbrace{\frac{1}{\lambda}\left[\overline{f(C_{kk}+c_{kk})(C_{kk}+c_{kk})}-f(L)\delta_{ij}\right]}_{\overline{\tau}_{ij,p}/\eta_p} \tag{8}$$

Here, the first term on the left hand side is the mean flow advective transport of C_{ij} which vanishes for fully developed channel flow, CT_{ij} is the contribution to the advective transport of the conformation tensor by the fluctuating velocity and conformation fields, M_{ij} is the mean flow distortion term of the Oldroyd derivative of C_{ij}, and NLT_{ij} accounts for the interactions between the fluctuating components of the conformation tensor and of the velocity gradient tensor. This term also originates from the distortion term of the Oldroyd derivative and is the fluctuating counterpart of M_{ij}.

2.3. Reynolds stresses

To calculate the Reynolds stress tensor in Eq. (4) Boussinesq's turbulent stress–strain relationship was adopted:

$$-\rho\overline{u_i u_j}=2\rho\nu_T S_{i_j}-\frac{2}{3}\rho k\delta_{ij} \tag{9}$$

where υ_T is the eddy viscosity and k is the turbulent kinetic energy, $\overline{u_i u_i}/2$. In this work as in [15] the eddy viscosity is modeled according to the $k-\varepsilon-\overline{v^2}-f$ model of Durbin et al. [23,24]. This particular choice is because of the capability of this turbulence model in calculating accurately the turbulence statistics in wall bounded flows without introducing the wall-distance or low-Reynolds number damping functions. In this model the eddy viscosity is calculated as:

$$v_T = C_\mu \overline{v^2} T_t \tag{10}$$

where C_μ is the constant coefficient, $\overline{v^2}$ is the wall normal Reynolds stress, and T_t is the turbulent time scale defined as:

$$T_t = \max\left\{\frac{k}{\varepsilon}, 6\sqrt{\frac{\upsilon}{\varepsilon}}\right\} \tag{11}$$

This model is an extension of the k–ε model, and requires solving two extra equations for $\overline{v^2}$, and f along with the k and ε equations. The extended transport equations for the turbulent kinetic energy and its dissipation rate appropriate to deal with the FENE-P fluids in the context of the $k-\varepsilon-\overline{v^2}-f$ model were presented in [15] and are given by Eqs. (12) and (13). Note that both the k and ε equations contain additional terms in order to account for viscoelasticity,

$$U_j\frac{\partial k}{\partial x_j} = P_{kk} - \varepsilon + \frac{\partial}{\partial x_j}\left(\left(v+\frac{v_T}{\sigma_k}\right)\frac{\partial k}{\partial x_j}\right) - \left(\overline{\tau_{ij}^p \frac{\partial u_i}{\partial x_j}}\right) + \frac{\partial}{\partial x_j}\left(\overline{\tau_{ij}^p u_i}\right) \tag{12}$$

$$U_j\frac{\partial \varepsilon}{\partial x_j} = \frac{C_{\varepsilon 1}P_{kk} - C_{\varepsilon 2}\varepsilon}{T_t} + \frac{\partial}{\partial x_j}\left(\left(v+\frac{v_T}{\sigma_\varepsilon}\right)\frac{\partial \varepsilon}{\partial x_j}\right) - E_p \tag{13}$$

Here, all terms are conceptually identical to those for a Newtonian fluid except for the last two terms in the turbulent kinetic energy equation, Eq. (12), and the term E_p in the dissipation equation. In the former equation they represent the viscoelastic turbulent transport $\left(Q_p \equiv \partial\left(\overline{\tau_{ij}^p u_i}\right)/\partial x_j\right)$, and the viscoelastic stress work $\left(\varepsilon_p \equiv \overline{\tau_{ij}^p \partial u_i/\partial x_j}\right)$, whereas in the latter equation the new term (E_p) accounts for the viscoelastic contribution to the transport equation of ε.

The other two equations required to compute the eddy viscosity are the transport equation for the scalar $\overline{v^2}$, which is derived from the transport equation for the wall normal turbulent fluctuations according to [15], and the equation for the turbulence energy redistribution process, f. As discussed in [15] the equations for $\overline{v^2}$ and f appropriate for the FENE-P fluids are given by:

$$U_j\frac{\partial \overline{v^2}}{\partial x_j} = kf + \frac{\partial}{\partial x_j}\left(\left(v+\frac{v_T}{\sigma_k}\right)\frac{\partial \overline{v^2}}{\partial x_j}\right) - 6\frac{\varepsilon}{k}\overline{v^2} - \varepsilon_{p,v2} + Q_{p,v2} \tag{14}$$

$$f - L_t^2\frac{\partial^2 f}{\partial x_j \partial x_j} = \frac{1}{T_t}\left(\frac{2}{3}(C_1-1) - (C_1-6)\frac{\overline{v^2}}{k}\right) + C_2\frac{P_{kk}}{k} \tag{15}$$

where L_t is a length scale accounting for turbulence and wall proximity defined as:

$$L_t^2 = C_L^2 \max\left\{\frac{k^3}{\varepsilon^2}, C_\eta^2\sqrt{\frac{v^3}{\varepsilon}}\right\} \tag{16}$$

As reported in [24] the values of the coefficients appearing in the above equations are listed in Table 3. $C_\mu = 0.19$, $\sigma_k = 1$, $\sigma_\varepsilon = 1.3$, $C_{\varepsilon 1} = 1.4\left[1+0.05\sqrt{k/\overline{v^2}}\right]$, $C_{\varepsilon 2} = 1.9$, $C_1 = 1.4$, $C_2 = 0.3$, $C_L = 0.23$, $C_\eta = 70$.

2.4. Energy equation

The instantaneous thermal energy equation for incompressible flow can be written as,

$$\frac{\partial T}{\partial t} + u_j\frac{\partial T}{\partial x_j} = \frac{K}{\rho C_p}\frac{\partial^2 T}{\partial x_j^2} \tag{17}$$

The thermal boundary condition of uniform heat flux at both walls is considered in this study to which corresponds a linear variation of the wall temperature in thermally fully-developed flow [25]. To impose the periodic boundary condition for temperature, the temperature is made dimensionless as following,

$$\theta^+ = \frac{\langle T_w\rangle - T}{T^*}, \quad T^* = \frac{q''}{\rho C_p U_m} \tag{18}$$

Using the normalized temperature (temperature is normalized by the friction temperature), the non-dimensional governing equation (Eq. (19)) becomes the same as in Kasagi et al. [26].

$$\frac{\partial \theta^+}{\partial t} + u_j\frac{\partial \theta^+}{\partial x_j} - \frac{u_1}{U_m} = \frac{1}{Re_\tau Pr}\frac{\partial^2 \theta^+}{\partial x_j^2} \tag{19}$$

In Eq. (19) U_m represents the bulk mean velocity; Pr denotes the molecular Prandtl number, defined as the ratio of kinematic viscosity to thermal diffusivity. By Reynolds averaging Eq. (19) the thermal field is obtained by,

$$\frac{D\Theta^+}{Dt} - \frac{\overline{u_1}}{U_m} = \frac{1}{Re_\tau Pr}\frac{\partial^2 \Theta^+}{\partial x_j^2} - \frac{\partial \overline{u_j\theta'^+}}{\partial x_j} \tag{20}$$

In this equation $\overline{u_j\theta'^+}$ is the thermal flux, which is non-linear and requires a closure.

3. DNS of heat transfer of viscoelastic dilute polymer solutions

3.1. Computational and physical parameters

The fully developed channel flow of FENE-P fluids over a wide range of rheological and flow properties is investigated and the DNS cases studied are summarized in Table 1. A semi-implicit method is used for time-integration of the governing equations. In space, a spectral method is used with Fourier representations in the streamwise and spanwise directions, and Chebyshev expansion in the wall-normal direction. To achieve stable numerical integration a stress diffusion term is introduced. As in earlier studies [12,15], the dimensionless artificial numerical diffusivity is taken to be $O(10^{-2})$. Periodic boundary conditions are applied in the streamwise (x) and spanwise (z) directions, and the no-slip boundary condition is imposed on velocity at the solid walls. Details of the numerical approaches used in this work can be found in [12].

It is known that the smallest scales of the instantaneous temperature field decrease with the Prandtl number, in inverse proportion to $Pr^{1/2}$, [26]. Therefore, for the simulation of the thermal field with high Prandtl number fluids, the mesh should be finer than the requirement for the velocity field only. To solve the energy equation, Eq. (19) is discretized in time with second-order temporal accuracy. Details of the numerical methods for solving thermal field in this work can be found in [13]. Table 2 lists the simulations of heat transfer of FENE-P fluid flows for all cases studied here.

3.2. Time-averaged statistics

The mean temperature profiles for the viscoelastic and Newtonian cases corresponding to $Re_\tau = 180$, $Pr = 1.25$ and $Re_\tau = 125$, $Pr = 5$ are plotted in Figs. 1 and 2, respectively. As expected, the figures show that near the wall all the mean temperature profiles collapse on the linear distribution: $y^+ = Pr\Theta^+$, regardless of the

Table 1
Summary of the physical and computational parameters for the DNS of fluid flow.

Case	$Re_{\tau 0}$	Domain size $L_x \times L_y \times L_z$	Nodes $N_x \times N_y \times N_z$	L^2	$Wi_{\tau 0}$	β
(1)	125	6.283 h × 2 h × 3.141 h	96 × 97 × 96	0	0	0
(2)	180	6.283 h × 2 h × 3.141 h	128 × 129 × 128	0	0	0
(3)	395	14.136 h × 2 h × 4.5 h	384 × 257 × 192	0	0	0
(4)	590	14.136 h × 2 h × 4.5 h	512 × 257 × 256	0	0	0
(5)	125	6.944 h × 2 h × 4.19 h	96 × 97 × 96	900	25	0.9
(6)	125	6.944 h × 2 h × 4.19 h	96 × 97 × 96	900	50	0.9
(7)	125	6.944 h × 2 h × 4.19 h	96 × 97 × 96	900	100	0.9
(8)	125	6.944 h × 2 h × 4.19 h	96 × 97 × 96	3600	25	0.9
(9)	125	6.944 h × 2 h × 4.19 h	96 × 97 × 96	3600	50	0.9
(10)	125	6.944 h × 2 h × 4.19 h	96 × 97 × 96	3600	100	0.9
(11)	125	6.944 h × 2 h × 4.19 h	96 × 97 × 96	14,400	25	0.9
(12)	125	6.944 h × 2 h × 4.19 h	96 × 97 × 96	14,400	50	0.9
(13)	180	6.944 h × 2 h × 4.19 h	128 × 129 × 128	900	25	0.9
(14)	180	13.888 h × 2 h × 4.19 h	128 × 129 × 128	900	50	0.9
(15)	180	13.888 h × 2 h × 4.19 h	128 × 129 × 128	900	100	0.9
(16)	180	13.888 h × 2 h × 4.19 h	128 × 129 × 128	3600	50	0.9
(17)	180	13.888 h × 2 h × 4.19 h	128 × 129 × 128	3600	100	0.9
(18)	395	14.136 h × 2 h × 4.5 h	384 × 129 × 128	900	25	0.9
(19)	395	14.136 h × 2 h × 4.5 h	384 × 257 × 192	900	100	0.9
(20)	395	14.136 h × 2 h × 4.5 h	384 × 257 × 192	3600	75	0.9
(21)	395	14.136 h × 2 h × 4.5 h	384 × 257 × 192	14,400	75	0.9
(22)	395	14.136 h × 2 h × 4.5 h	384 × 257 × 192	3600	100	0.9
(23)	395	14.136 h × 2 h × 4.5 h	384 × 257 × 192	3600	50	0.9
(24)	590	25.136 h × 2 h × 4.5 h	512 × 257 × 256	3600	50	0.9
(25)	590	25.136 h × 2 h × 4.5 h	512 × 257 × 256	10,000	100	0.9

Table 2
Summary of the physical and computational parameters for the DNS of fluid flow with heat transfer.

Case	$Re_{\tau 0}$	Domain size $L_x \times L_y \times L_z$	Nodes $N_x \times N_y \times N_z$	L^2	$Wi_{\tau 0}$	β	Pr	$Dr.$ (%)
(H0)	125	10 h × 2 h × 5 h	128 × 97 × 257	0	0	0	5.0	0
(H1)	180	10 h × 2 h × 5 h	128 × 129 × 128	0	0	0	1.25	0
(H2)	180	10 h × 2 h × 5 h	128 × 129 × 128	900	25	0.9	1.25	18.5
(H3)	180	10 h × 2 h × 5 h	128 × 129 × 128	3600	75	0.9	1.25	50
(H4)	125	10 h × 2 h × 5 h	128 × 97 × 257	900	25	0.9	5.0	18.5
(H5)	125	10 h × 2 h × 5 h	128 × 97 × 257	900	100	0.9	5.0	37
(H6)	125	10 h × 2 h × 5 h	128 × 97 × 257	3600	100	0.9	5.0	56.5

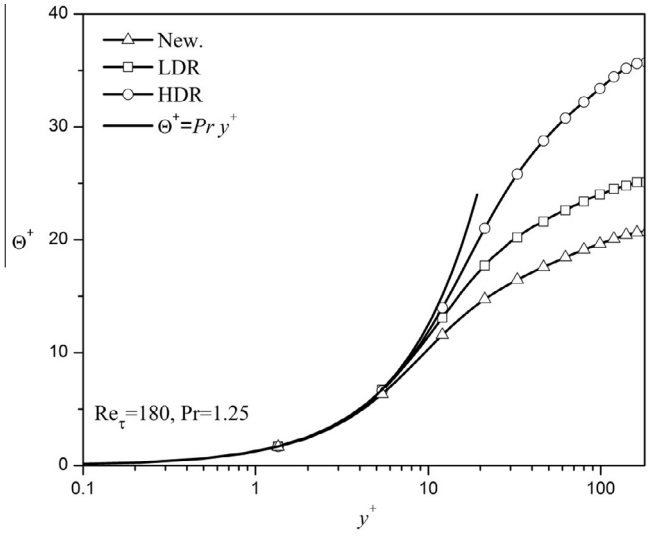

Fig. 1. Profiles of mean temperature in wall coordinates calculated by DNS for Newtonian (New: H1) and viscoelastic (LDR: H2, HDR: H3) fluid flows. Flow and rheological parameters are described in Table 2.

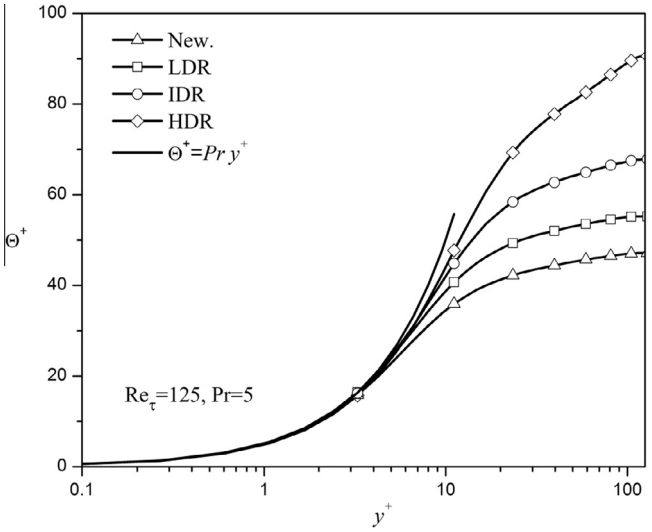

Fig. 2. Profiles of mean temperature in wall coordinates calculated by DNS for Newtonian (New: H0) and viscoelastic (LDR: H4, IDR: H5, HDR: H6) fluid flows. Flow and rheological parameters are described in Table 2.

amount of Re_τ, Pr, L^2, and Wi_τ. Further away from the wall the mean temperature profiles of the drag reduced flows increases as compared to that of Newtonian flows regardless of the amount of Re_τ, and Pr numbers, in essence as expected the temperature profiles bear a qualitative similarity to the corresponding velocity profiles in wall coordinates. These figures further indicate that the conduction region penetrates more deeply into the core region with increase of amount of drag reduction.

Figs. 3 and 4 show that although the overall shape of the temperature fluctuation intensity for the viscoelastic flows remains the same as for the Newtonian case, the maximum temperature fluctuation intensity increases and shifts toward the bulk flow region as DR increases. For instance, the maximum temperature fluctuation intensity for the high drag reduction case corresponding to $Re_\tau = 125$, $Pr = 5$, is around 14.6, whereas for the Newtonian case is around 8.2.

The streamwise turbulent heat flux for all cases are plotted in Figs. 5 and 6, and we observe an enhancement of this flux with drag reduction, as previously reported by Gupta et al. [13], Yu and Kawaguchi [14]. In addition, by increasing the Pr number streamwise heat flux is enhanced for both Newtonian and viscoelastic cases.

The wall normal turbulent heat flux and the conductive heat flux for the Newtonian and high drag reduction flow cases are compared in Fig. 7. As can be observed, unlike the streamwise turbulent heat flux, the wall normal heat flux for viscoelastic fluids is decreasing, comparing with Newtonian case. For the viscoelastic flow a shift in the peak location toward the bulk flow can also be observed. Moreover, the figure shows that the conductive heat flux compensates for the decrease of wall-normal heat flux, meaning the importance of conduction in viscoelastic fluids, particularly at high drag reduction regimes.

It is well known that the thermal structures closely resemble the velocity fields structures, i.e. high and low temperature structures are associated with high and low velocity regions, respectively. In Fig. 8 the iso-surfaces of the instantaneous temperature field for Newtonian, low and high drag reduction cases are depicted. As can be observed from the figure the thermal structures become elongated and highly organized by increasing the amount of drag reduction, typical characteristics of polymer dilute solutions. Note that for all cases in Fig. 8 the threshold of iso-surfaces is 75% of the mean centerline temperature.

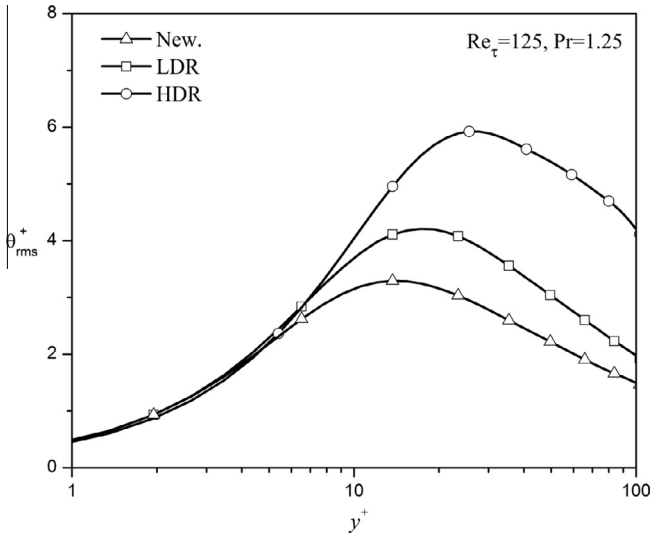

Fig. 3. Profiles of root mean square of temperature fluctuation in wall coordinates for Newtonian (New: H1) and viscoelastic (LDR: H2, HDR: H3) fluid flows. Flow and rheological parameters are described in Table 2.

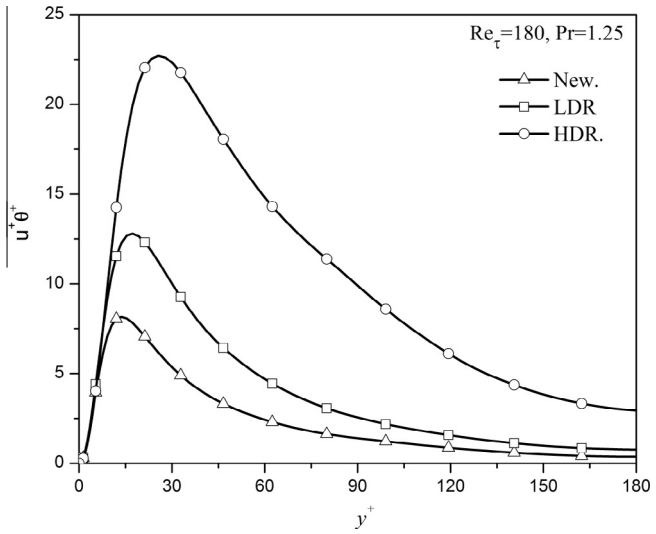

Fig. 5. Transverse profiles of streamwise turbulent heat flux for Newtonian (New: H1) and viscoelastic (LDR: H2, HDR: H3) fluid flows. Flow and rheological parameters are described in Table 2.

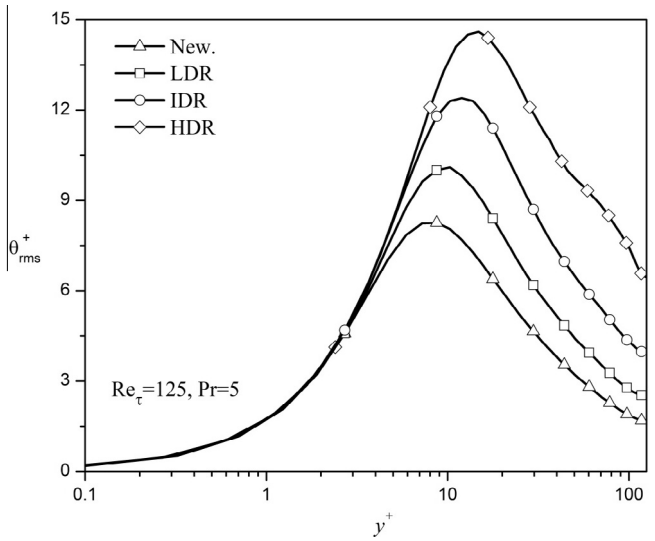

Fig. 4. Profiles of root mean square of temperature fluctuation in wall coordinates for Newtonian (New: H0) and viscoelastic (LDR: H4, IDR: H5, HDR: H6) flows. Flow and rheological parameters are described in Table 2.

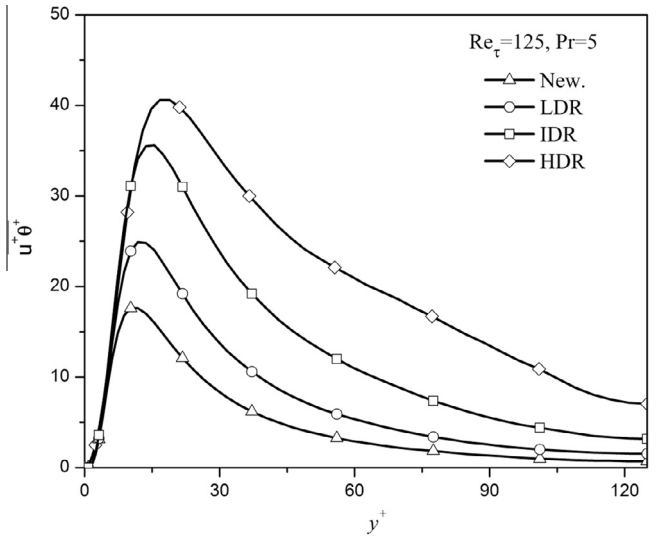

Fig. 6. Transverse profiles of streamwise turbulent heat flux for Newtonian (New: H0) and viscoelastic (LDR: H4, IDR: H5, HDR: H6) fluid flows. Flow and rheological parameters are described in Table 2.

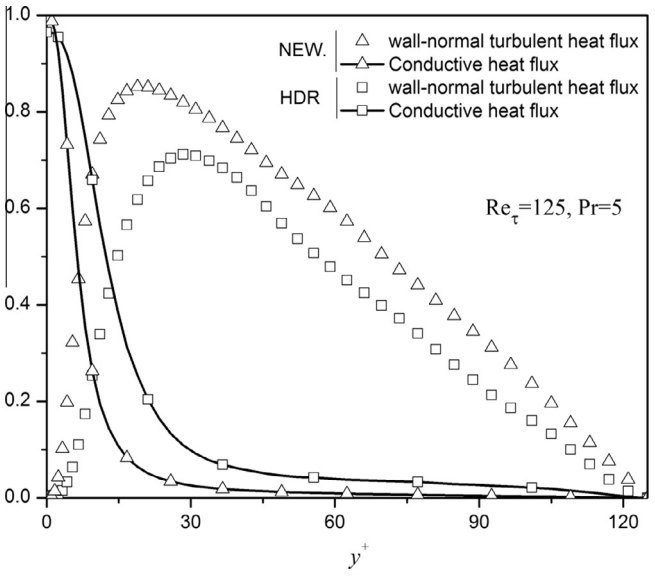

Fig. 7. Transverse profiles of the budget of heat flux for Newtonian (New: H0) and viscoelastic (HDR: H6) cases. Flow and rheological parameters are described in Table 2.

The budget of the transport equation of the temperature variance for Newtonian, low and high drag reduction cases are plotted in Fig. 9. By adding polymer to the flow although the overall shape and behavior of the different terms remains the same as for the Newtonian case, the magnitude and location of the peak values are influenced by the additives and the amount of drag reduction. In particular, by increasing the amount of drag reduction the peak location of all terms shifts toward the bulk flow region. This shift of the peak location can be interpreted as a thickening of the buffer layer.

4. Development of the closures

First, we discuss the improvements in the model for predicting the isothermal flow and subsequently, in Section 4.3, we discuss the closures required for the heat transfer Reynolds flux.

4.1. Improvement of conformation tensor closures

The first term that needs closure is the time-averaged polymer stress, Eq. (4). The expanded form of the time-averaged polymer stress is given by,

$$\overline{\tau}_{ij,p} = \frac{\eta_p}{\lambda}\underbrace{\left[f(C_{kk})C_{ij} - f(L)\delta_{ij}\right]}_{term1} + \frac{\eta_p}{\lambda} \times \underbrace{\left[\overline{f(C_{kk}+c_{kk})(C_{ij}+c_{ij})} - f(C_{kk})C_{ij}\right]}_{term2} \tag{21}$$

Both terms on the right-hand-side of Eq. (21) were evaluated in [15,19] by using *a priori* DNS data at different values of $Wi_{\tau 0}$ and L^2, and it was shown that the first term, which is exact, is nearly 20 times larger than the second term regardless of the rheological parameters. Consequently, here as in [15,19], $\overline{\tau}_{ij,p}$ is approximated as the first term on the right hand side of Eq. (21), and the second term is neglected, hence the Reynolds-averaged polymer stress will be calculated by:

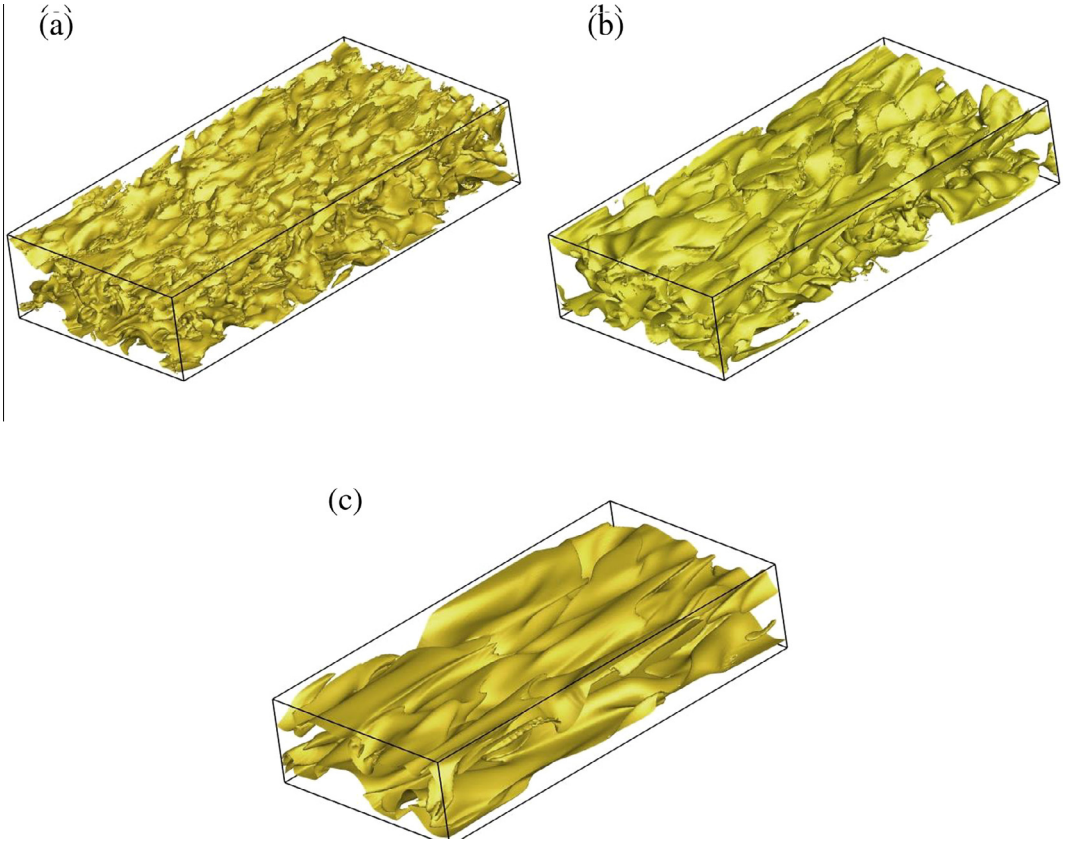

Fig. 8. Iso-surfaces of the instantaneous temperature field for (a): Newtonian flow (case H1), (b): low drag reduction flow (H2) and (c): high drag reduction flow (H3). Note that the same threshold (75% of mean centerline temperature) was utilized for visualization of all cases.

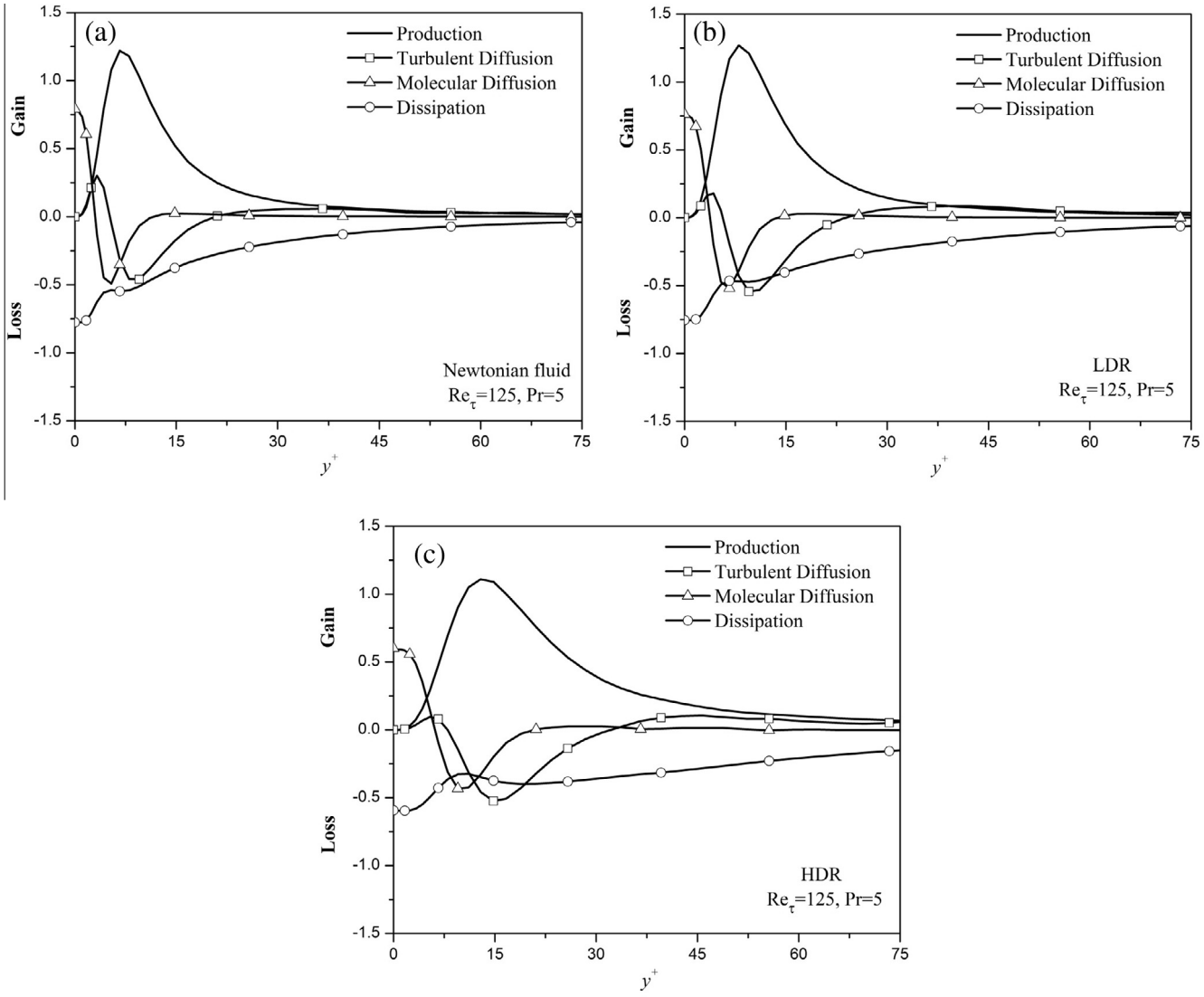

Fig. 9. Budget terms of temperature variance. (a) Newtonian fluid (H0), (b) low drag reduction case (H4) (c) high drag reduction case (H6).

$$\overline{\tau}_{ij,p} = \frac{\eta_p}{\lambda}\left[f(C_{kk})C_{ij} - f(L)\delta_{ij}\right] \tag{22}$$

To compute the polymer stress using Eq. (22) we need the components of the conformation tensor, C_{ij}, and these can be computed directly via the corresponding Reynolds-averaged equation, Eq. (8). In Eq. (8) all terms are exact except for NLT_{ij}, which is the fluctuating counterpart of M_{ij}, and CT_{ij}, which is discarded for being negligible as shown in [27].

Previous attempts at developing closures for NLT_{ij} in the context of $k-\varepsilon-\overline{v^2}-f$ [15] were based on a simplified representation of the polymer conformation tensor. In particular, they only considered the extension of the chains as characterized by the trace of the C_{ij} tensor, and a separate closure was proposed for the shear component of NLT_{ij} based on the concept of viscoelastic turbulent viscosity to account for the polymer shear stress, the only stress component relevant in fully-developed turbulent channel flow. The complete form of the Reynolds-averaged FENE-P constitutive equation and its exact solution appears in the Appendix A of [16].

Since NLT_{kk} accounts for the interactions between the fluctuating components of the conformation tensor and of the velocity gradient tensor, and it is the fluctuating counterpart of M_{ij}, Masoudian et al. [15] developed a model for the trace of NLT_{ij} as a function of its mean value (M_{kk}) and the eddy viscosity given by:

$$NLT_{kk} = a_{NLT}M_{kk}\frac{\nu_T}{\nu_o}, \quad a_{NLT} = 0.16 \tag{23}$$

In this work a general form of closure developed in [15] is proposed by using a Boussinesq like relationship to account for the influence of NLT_{ij} upon polymer chain extension and orientation via:

$$NLT_{ij} = a_{NLT}\sqrt{L^2}M_{ij}\frac{\nu_T}{\nu_o}, \quad a_{NLT} = 0.04 \tag{24}$$

As it can be seen only the square root of the dimensionless polymer maximum extension coefficient is added here to the closure of [15]. This particular change in the closure for NLT_{ij} was based on a numerical optimization procedure using our DNS database listed in Table 1 with the objective function defined as a minimum error in the prediction of drag reduction. In Fig. 10(a) this optimized closure is evaluated and compared with the DNS results and with the predictions by the previous closure of [15]. As it can be observed from Fig. 10(a) the new closure is in good agreement with the DNS results and performs better than the previous closure. Furthermore, in order to examine the performance of the optimized closure, two sets of DNS data with different rheological properties were used. These two sets have not been used in the optimization process of closure development and their characteristics are: case

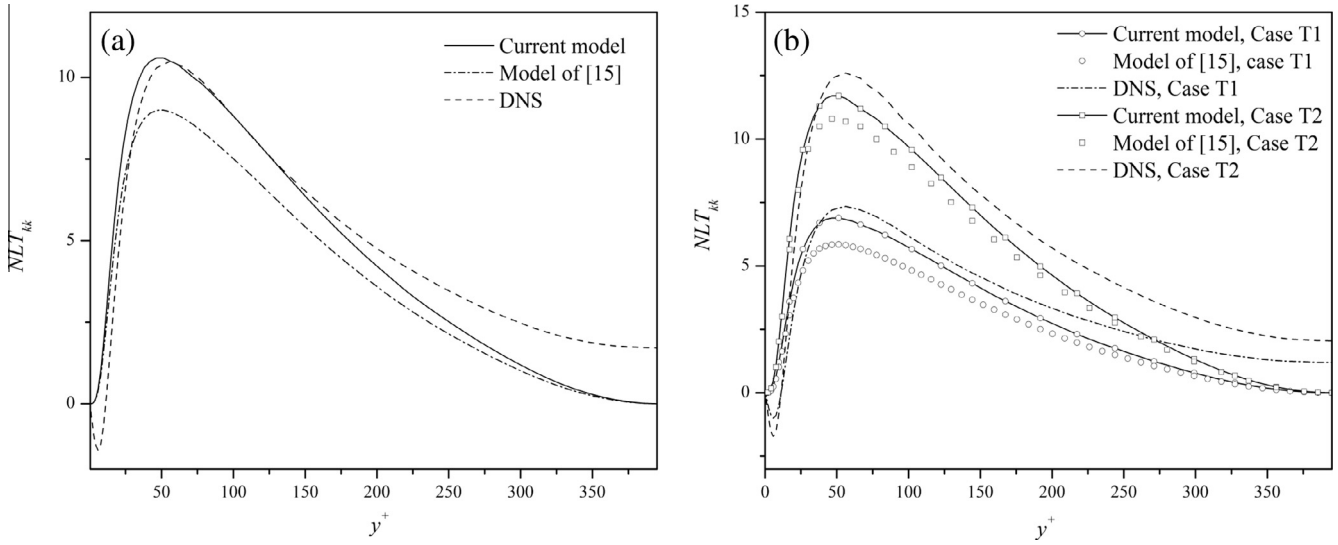

Fig. 10. Comparison between predicted and DNS data for NLT_{kk} (a) case (19), (b) cases T1 and T2.

T1 $Re_{\tau 0} = 395$, $Wi_{\tau 0} = 75$, $L^2 = 900$, and case T2 $Re_{\tau 0} = 395$, $Wi_{\tau 0} = 25$, $L^2 = 3600$. In Fig. 10(b) this closure is evaluated and compared with DNS data for cases T1 and T2.

The prediction of the mean polymer extension using the new closure is assessed against DNS data in Fig. 11, showing again a good agreement with DNS results. It is worth mentioning that, since the polymer stress work in the turbulent kinetic energy equation, as described in [15], is a direct function of NLT_{kk}, the current improvement in the prediction of NLT_{kk} will benefit the prediction of turbulent kinetic energy.

The extensive analysis of the performance of the closure will be presented in the results section, and comparison with the DNS data for a wide range of the rheological and flow parameters will be shown. It is worth mentioning that using this model the Reynolds averaged conformation tensor can be calculated now only by using one single constant coefficient which shows the robustness of the present model compared to the previous attempts in this context, all of which need more than one constant coefficient and *ad hoc* damping functions.

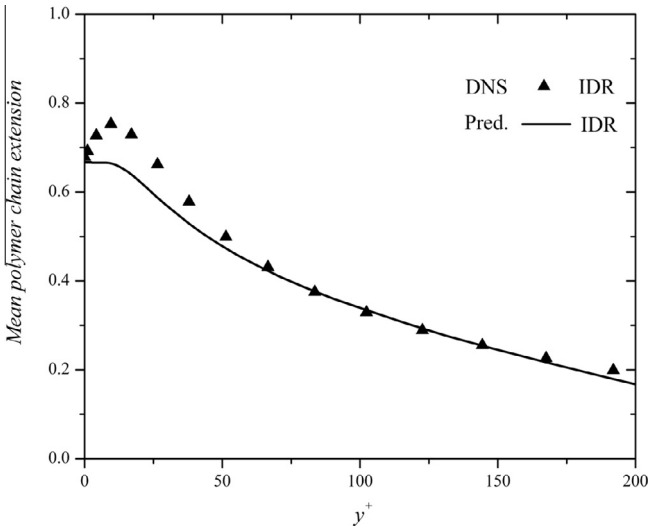

Fig. 11. Comparison between mean polymer extension and DNS data for case (19).

4.2. Improvements of closures needed by the V2F model

As emphasized, the turbulent kinetic energy and dissipation transport equations contain viscoelastic nonlinear terms, which require modeling. The viscoelastic terms appearing in the turbulent kinetic energy and dissipation equations were modeled using their exact definitions in [15] and the closures tested for a wide range of rheological and flow parameters. There, it was demonstrated that those closures are robust enough to accurately account for the influence of viscoelasticity upon kinetic energy and its dissipation rate, hence they are used here unmodified.

However, the closure of the term accounting for the polymer influence in the transport equation of $\overline{v^2}$, is optimized to improve predictions of the wall normal Reynolds stress. Comparing with the corresponding closure developed in [15] only the constant coefficient and the power exponent of the Peterlin function, which accounts for the influence of the polymer chain extension, are changed. The updated closure is given by,

$$\varepsilon_{p,v2} = a_{v2} L [f(C_{kk})]^2 kf, \quad \text{with} \quad a_{v2} = 0.002 \tag{25}$$

The predictions of k and $\overline{v^2}$ are plotted and compared with DNS and with the previous closures in Fig. 12 for the intermediate drag reduction case (IDR). The new predictions of k and $\overline{v^2}$ are in good agreement with DNS data and compare better than those of the previous model of [15]. The predictions of Reynolds shear stress and mean streamwise velocity for the same IDR case are assessed in Figs. 13 and 14, respectively. Both figures show that the model is capable of predicting well both the Reynolds shear stress and the mean velocity. This particular modification in the closure of the viscoelastic term in the $\overline{v^2}$ equation was performed because of the failure of the previously developed closure [15] in predicting high drag reduction flows at very low Reynolds numbers, namely at $Re_{\tau 0} = 125$, for which the wall normal Reynolds stress is very small. In fact the calculation of high drag reduction flows at low Reynolds numbers using the closure of [15] leads to a complete laminarization of the flow. Extensive analyses of the performance of the closure will be presented in the result section.

4.3. Reynolds scalar flux model for viscoelastic fluids

The turbulent thermal energy flux term, $\overline{u_j \theta'^+}$, appearing in the time-averaged energy equation is non-linear and requires a closure

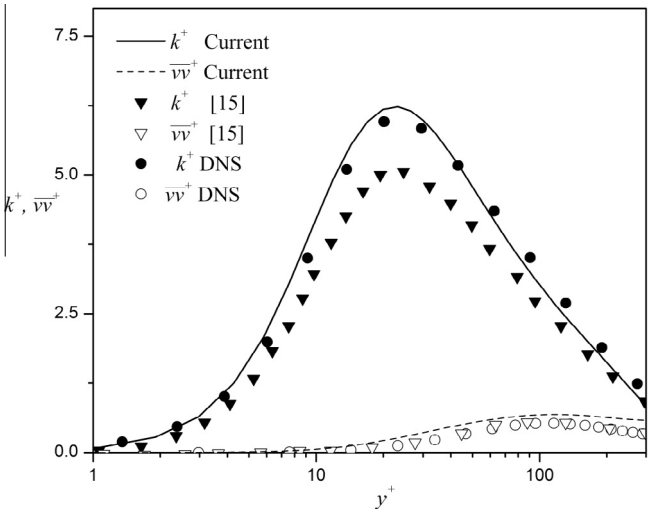

Fig. 12. Comparison between predicted and DNS data of k^+, $\overline{v^2}$ for case (19).

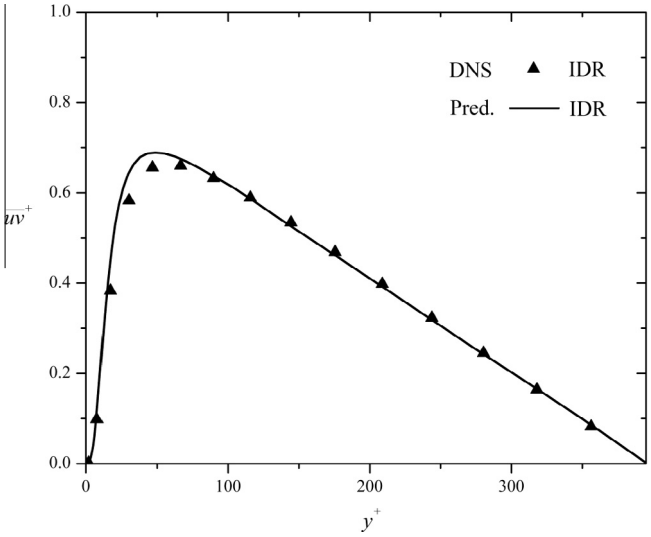

Fig. 13. Comparison between predicted and DNS data of Reynolds shear stress for case (19).

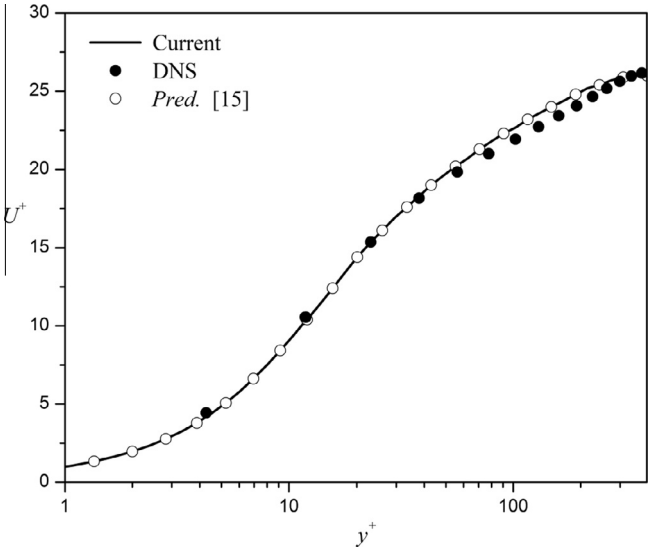

Fig. 14. Comparison between predicted and DNS data of mean streamwise velocity profile for case (19).

to allow computations of heat transfer. A common and simple way to model the thermal flux within the RANS approach is by using the concept of turbulent thermal diffusivity leading to,

$$\overline{u_j\theta'} = \alpha_t \frac{d\Theta}{dx_j} \tag{26}$$

where the turbulent thermal diffusivity, α_t, is expressed as a function of the eddy viscosity and a turbulent Prandtl number,

$$\alpha_t = \frac{v_t}{Pr_t} \tag{27}$$

In this relation the eddy viscosity is available from the flow turbulence model, so the only unknown quantity is the turbulent Prandtl number. In order to have an idea about how α_t is influenced by the presence of polymer additives, in Fig. 15(a) the ratios $\alpha_{viscoelastic}/\alpha_{Newtonian}$ and $v_{T,viscoelastic}/v_{T,Newtonian}$ are plotted for $Pr = 1.25$ using DNS data for low and high drag reduction cases. The figure shows that, as expected, the turbulent thermal diffusivity and turbulent viscosity are decreased by addition of polymers to the flow. Moreover, it is interesting to note that the ratio of turbulent thermal diffusivities nearly collapse on the ratio of turbulent viscosities, regardless of the amount of drag reduction, indicating that the closures developed for turbulent Prandtl number in the context of Newtonian fluids can be extended to viscoelastic fluids. These ratios plotted for high Prandtl number cases in Fig. 15(b), show the same trend as at low Prandtl numbers. In this work we adapted one of the commonest closures for the turbulent Prandtl number introduced by Kays [20], which is based only on the local quantities as a function of the turbulent Peclet number,

$$Pr_t = 0.85 + \frac{0.7}{Pe_t}, \quad \text{where} \quad Pe_t = \frac{v_T}{v} Pr \tag{28}$$

Using this closure the energy equation was solved and the mean temperature profiles are plotted in Fig. 16 for cases H2 and H3, cf. Table 2. As shown, the original model of Kays [20] under-predicts the mean temperature for the FENE-P fluids, and shows that the approximation of Eq. (28) is no longer valid. As discussed above the thermal turbulent diffusivity, α_t, decreases by increasing DR, and to capture the variation of α_t for viscoelastic fluids based on the *a priori* DNS data analyses, the following equation extending Kays' closure [20] for the turbulent Prandtl number is proposed,

$$Pr_{t,extended} = Pr_{t,Kays}\left(1 + \frac{a_p v_{T,viscoelastic}}{v_T}\right) \tag{29}$$

In this equation $v_{T,viscoelastic}$ is the viscoelastic turbulent viscosity defined as: $v_{T,viscoelastic} = \frac{\tau_{xy,p}}{2\rho S_{xy}}$, and the coefficient a_p is equal to 2.6 (this was quantified based on an iterative numerical optimization in order to achieve minimum error in predicting the mean temperature in comparison with DNS data).

The predictions of the mean temperature profiles using the extended closure are plotted in Fig. 16, and compared with DNS and predictions using Kays' [20] original closure for low and high drag reduction flows at $Pr = 1.25$. The figure clearly shows that the predictions using the extended closure are in good agreement with DNS results. Note that the modifications in Kays' turbulent Prandtl number closure were made based on the analysis of the low drag reduction and low Prandtl number case H2, Table 2. Its robustness is examined in the results section against DNS data for high Prandtl number cases from low to high drag reduction regimes.

4.4. Summary of the model and numerical method

Utilizing the closures developed in the previous section, the model equations are given below.

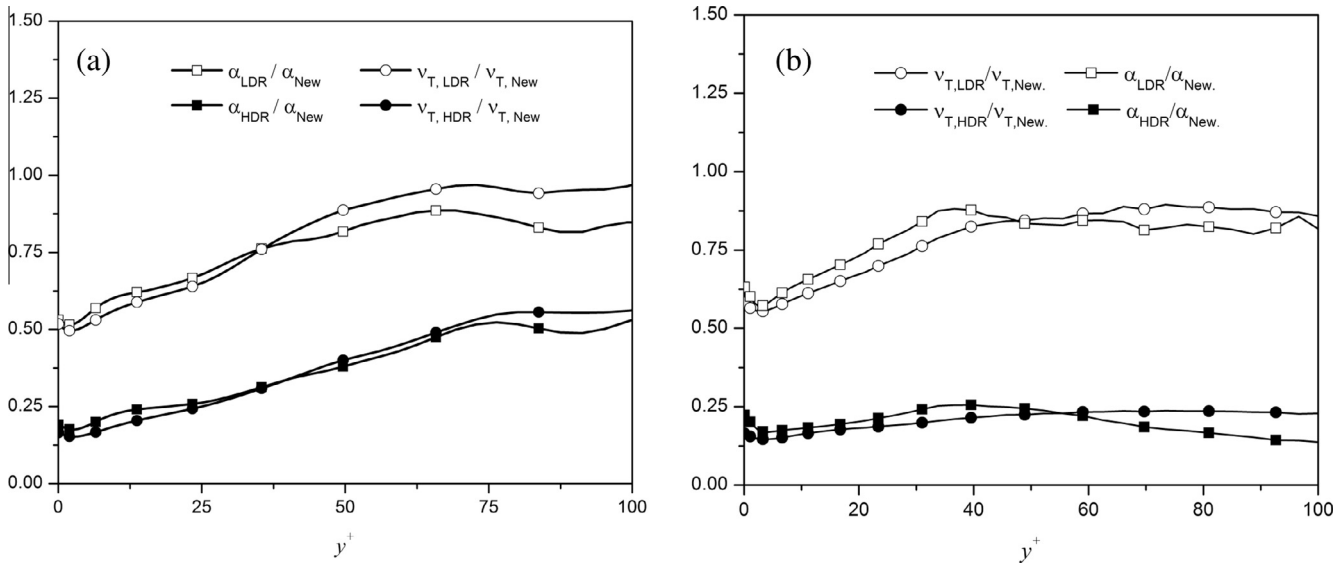

Fig. 15. Influence of viscoelasticity on turbulent thermal diffusivity, (a) low *Pr* number: (LDR: H2, HDR: H3), (b) high *Pr* number: (LDR: H4, HDR: H6).

$$\rho\frac{\partial U_i}{\partial t}+\rho U_k\frac{\partial U_i}{\partial x_k}=-\frac{\partial \overline{P}}{\partial x_i}-\frac{\partial}{\partial x_k}\rho(\overline{u_iu_k})+\frac{\partial \overline{\tau}_{ik}}{\partial x_k} \tag{30}$$

$$\frac{D\Theta^+}{Dt}-\frac{\overline{u_1}}{U_m}=\frac{1}{Re_\tau Pr}\frac{\partial^2\Theta^+}{\partial x_j^2}-\frac{\partial\overline{u_j\theta'^+}}{\partial x_j} \tag{31}$$

$$U_j\frac{\partial k}{\partial x_j}=P_{kk}-\varepsilon+\frac{\partial}{\partial x_j}\left(\left(\nu_s+\frac{\nu_T}{\sigma_k}\right)\frac{\partial k}{\partial x_j}\right)-\frac{\eta_p}{2\rho\lambda}f(C_{mm})NLT_{kk} \tag{32}$$

$$U_j\frac{\partial \varepsilon}{\partial x_j}=\frac{C_{\varepsilon1}P_{kk}-C_{\varepsilon2}\varepsilon}{T_t}+\frac{\partial}{\partial x_j}\left(\left(\nu_s+\frac{\nu_T}{\sigma_\varepsilon}\right)\frac{\partial \varepsilon}{\partial x_j}\right)-\frac{C_{\varepsilon1}\eta_p}{2\rho\lambda T_t}f(C_{mm})NLT_{kk} \tag{33}$$

$$U_j\frac{\partial\overline{v^2}}{\partial x_j}=kf+\frac{\partial}{\partial x_j}\left(\left(\nu_s+\frac{\nu_T}{\sigma_k}\right)\frac{\partial\overline{v^2}}{\partial x_j}\right)-6\frac{\varepsilon}{k}\overline{v^2}-a_{v2}L[f(C_{kk})]^2kf \tag{34}$$

$$f-L_t^2\frac{\partial^2 f}{\partial x_j\partial x_j}=\frac{1}{T_t}\left(\frac{2}{3}(C_1-1)-(C_1-6)\frac{\overline{v^2}}{k}\right)+C_2\frac{P_{kk}}{k} \tag{35}$$

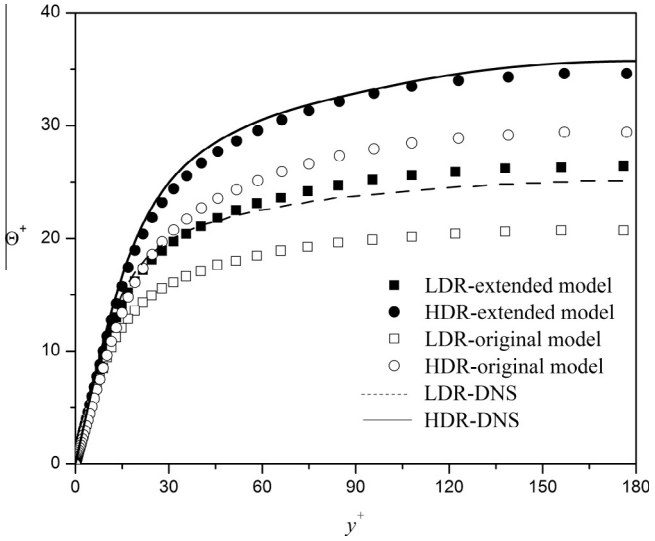

Fig. 16. Comparison between predicted and DNS data of mean temperature profile using the original and extended closure of Kays [20] for case (LDR: H2, HDR: H3).

$$U_k\frac{\partial C_{ij}}{\partial x_k}-M_{ij}-NLT_{ij}=-\frac{\overline{\tau}_{ij,p}}{\eta_p} \tag{36}$$

$$\overline{\tau}_{ij,p}=\frac{\eta_p}{\lambda}\left[f(C_{kk})C_{ij}-f(L)\delta_{ij}\right] \tag{37}$$

Coefficients arising from the Newtonian part of the model take on the same numerical values as reported in [24] and listed in Table 3.

The computer code used for the present model calculations is based on a finite-volume method using a second-order central difference scheme on a staggered mesh. The Tri-Diagonal Matrix Algorithm (TDMA) solver is used to calculate the solution of the discretized algebraic governing equations. The non-uniform mesh used in all simulations has 99 cells across the channel and it provides mesh independent results with 0.1% uncertainty in the amount of drag reduction prediction. The grid independency analyses for low and high drag reduction cases reported in Table 4 used consistently refined non-uniform meshes with 79 and 199 cells across the channel.

As mentioned above, in channel flow simulations we only need the trace and shear component of the conformation tensor, so only these components are solved. In order to stabilize the numerical simulation of the conformation tensor the quantity M_{kk} is calculated using the model of Iaccarino et al. [19]. The boundary conditions are those of no slip for the velocity, k and v^2, whereas for the dissipation by the solvent and f we use the standard conditions for Newtonian fluids described in [24]. The Dirichlet boundary condition introduced by Iaccarino et al. [19] is also utilized in this work to solve the conformation tensor equation.

Table 3
Coefficients of the developed RANS model.

Coefficient	Value
C_μ	0.19
σ_k	1.0
σ_ε	1.3
$C_{\varepsilon1}$	$1.4\left[1+0.05\sqrt{k/\overline{v^2}}\right]$
$C_{\varepsilon2}$	1.9
C_1	1.4
C_2	0.3
C_L	0.23
C_η	70.0

Table 4
Mesh independency analyses.

Case	Grid points across the channel	Predicted drag reduction (%)	DNS (%)
LDR	79	15.1	19
LDR	99	20	19
LDR	111	20	19
LDR	199	20	19
HDR	79	38	56
HDR	99	51	56
HDR	111	51	56
HDR	199	51	56

5. Results and discussions

In this section, predictions of fully-developed channel flow using this turbulence model are presented and assessed against DNS data for FENE-P fluids. All viscoelastic flow calculations were carried out using the same flow dimensionless numbers as for the DNS.

The predicted transverse profiles of the mean streamwise velocity for cases corresponding to low and high drag reductions (LDR, and HDR) are plotted in Fig. 17. The wall Reynolds number for all cases is 395, and the rheological parameters are listed in Table 1. All profiles in the viscous sublayer collapse on the linear distribution $U^+ = y^+$. Further away from the wall the mean velocity of the drag reduced flows increases as compared to that in Newtonian flows. Specifically in the LDR regime, the logarithmic profile is shifted upwards but remains parallel to that of the Newtonian flow as is also found in the DNS results. The upward shift of the logarithmic profile can be interpreted as a thickening of the buffer layer. As it can be observed the predictions and DNS are consistent regardless of the amount of drag reduction. Predictions by the previous closure of [15] are also included in Fig. 17, and as it can be seen the current model performs better.

The predicted profiles of k and $\overline{v^2}$ are compared with the DNS data and with the predictions of the previous model of [15] for LDR and HDR flows in Fig. 18(a) and (b), respectively. It is well known [12] that the turbulent kinetic energy monotonically increases with drag reduction and its peak location moves away from the wall as drag reduction increases, which is consistent with the upward shift of the logarithmic region in the mean velocity profile. This is observed when comparing Fig. 18 (a) and (b) and the current predictions improve significantly on the previous predictions approaching the DNS data, with the current model capturing both physical characteristics of turbulent channel flow of dilute polymer solutions in terms of an increase in k and the shift of its peak location with drag reduction. Nevertheless and in spite of the noticeable improvement on the prediction of k at high drag reduction, the current model still under-predicts its peak.

In contrast, by increasing drag reduction the Reynolds shear stress is significantly reduced in turbulent polymer dilute solution flows. The predicted Reynolds shear stress profiles are plotted in Fig. 19, normalized by the wall shear stress for low and high drag reductions and are in good agreement with the corresponding DNS data regardless of the amount of DR. The corresponding predictions of the mean polymer extension (C_{kk}/L^2) are compared with DNS data in Fig. 20 for LDR and HDR and again the agreement is good.

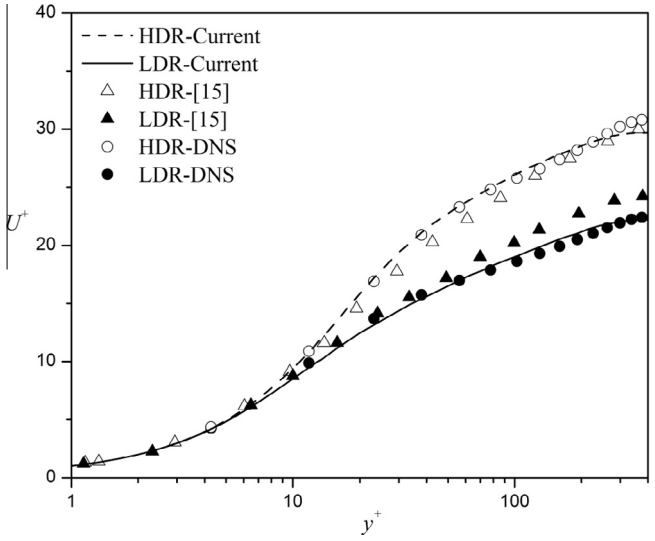

Fig. 17. Comparison between predicted and DNS data of mean streamwise velocity profile for low and high drag reduction cases, LDR (case 14) and HDR (case 18) respectively. Flow and rheological parameters are described in Table 1.

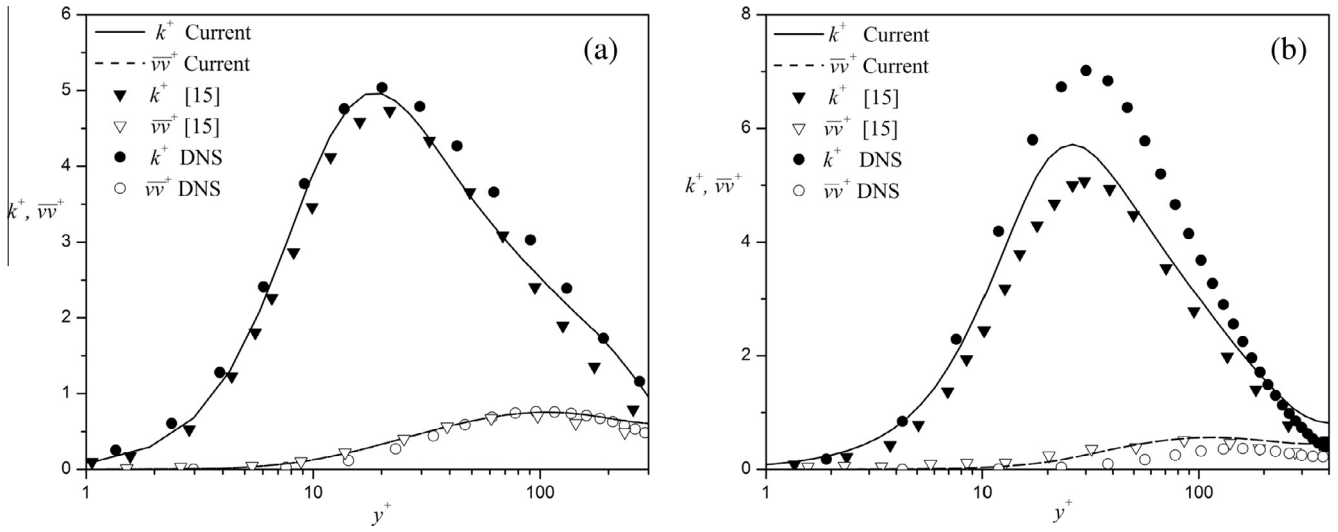

Fig. 18. Comparison between predicted and DNS data of k^+, $\overline{v^2}$ for (a) LDR: case 14, (b) HDR: case 18. Flow and rheological parameters are described in Table 1.

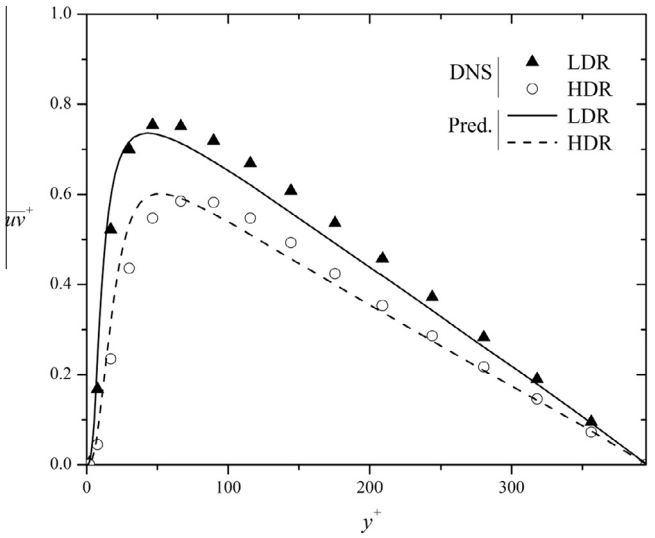

Fig. 19. Comparison between predicted and DNS data of Reynolds shear stresses for low (LDR: case 14) and high (HDR: case 18) drag reductions cases. Flow and rheological parameters are described in Table 1.

Table 5
Comparison of drag reduction prediction levels using current model.

Case	Reference	Flow and rheological properties			Drag reduction predictions	
		$Re_\tau = \frac{U_\tau h}{\nu_0}$	$Wi_\tau = \frac{U_\tau^2 \lambda}{\nu_0}$	L^2	DNS (%)	Model (%)
(1)	Li et al. [12]	125	25	900	20	19
(2)	Li et al. [12]	125	25	3600	22	22
(3)	Li et al. [12]	125	25	14,400	24	26
(4)	Li et al. [12]	125	50	900	31	31
(5)	Li et al. [12]	125	50	3600	43	39
(6)	Li et al. [12]	125	50	14,400	51	46
(7)	Li et al. [12]	125	100	900	37	37
(8)	Li et al. [12]	125	100	3600	56	51
(9)	Li et al. [12]	180	25	900	19	19
(10)	Li et al. [12]	180	50	900	31	30
(11)	Li et al. [12]	180	100	900	39	39
(12)	Li et al. [12]	180	100	3600	54	50
(13)	Iaccarino et al. [19]	300	36	10,000	35	34
(14)	Current DNS data	395	25	900	19	20
(15)	Current DNS data	395	50	900	30	29
(16)	Current DNS data	395	50	3600	38	38
(17)	Current DNS data	395	100	900	37	36
(18)	Current DNS data	395	100	3600	48	46
(19)	Current DNS data	395	100	14,400	61	58
(20)	Current DNS data	590	50	3600	39	38
(21)	Thais et al. [11]	1000	50	900	30	30

The present turbulence model compares well with DNS data in terms of overall drag reduction; a collection of representative calculations is reported in Table 5. In total 21 cases including current DNS data and independent DNS data are gathered and the performance of the model investigated. As it can be seen the wide range of Reynolds number ($125 < Re < 1000$) with different amount of drag reduction are tested to examine the robustness of the model. For the sake of comparison for three cases at different Reynolds numbers (cases 8, 9, 20) the predictions of the U^+, k^+ and $\bar{v}^2$ profiles are plotted in Figs. 21 and 22, respectively, and compared with the corresponding DNS data.

The predicted profiles of the mean temperature using the extended model of Kays [20] for cases H4, H5, and H6, corresponding to low, intermediate and high drag reductions (LDR, IDR, and HDR), are plotted in Fig. 23. The wall Reynolds number for all cases is 125, molecular Prandtl number is 5, and the rheological parameters are listed in Table 2. For all cases the fully-developed temperature profiles are in good agreement with the DNS data both close and far from the wall. As can be seen for all cases the model has an excellent performance close to the wall, and far from the wall, near the centerline its predictions differ by around 7% for high drag reduction case, H6. Although this difference is acceptable in the context of RANS, the main reason for this under prediction is related to the fact that near the channel center the assumption invoked in Section 4.3 has an error of around 10% (the ratio of turbulent thermal diffusivities differs from the ratio of turbulent viscosities by around 10%, as shown in Fig. 15(a) and (b)).

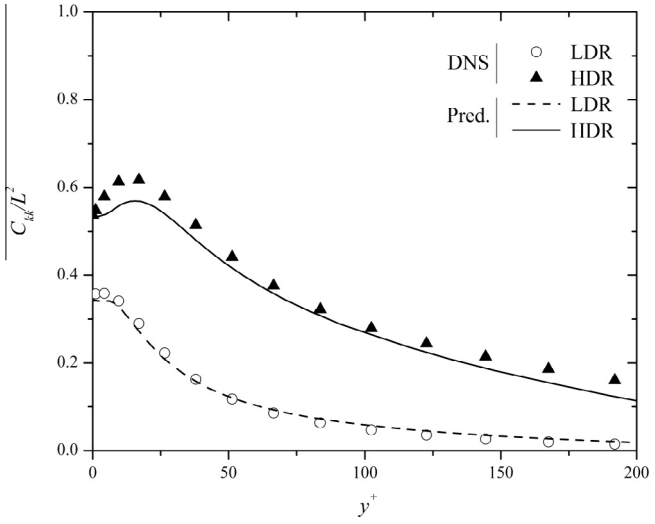

Fig. 20. Comparison between predicted and DNS data for the mean polymer extension at low (LDR) and high (HDR) drag reduction cases. Flow and rheological parameters are described in Table 1.

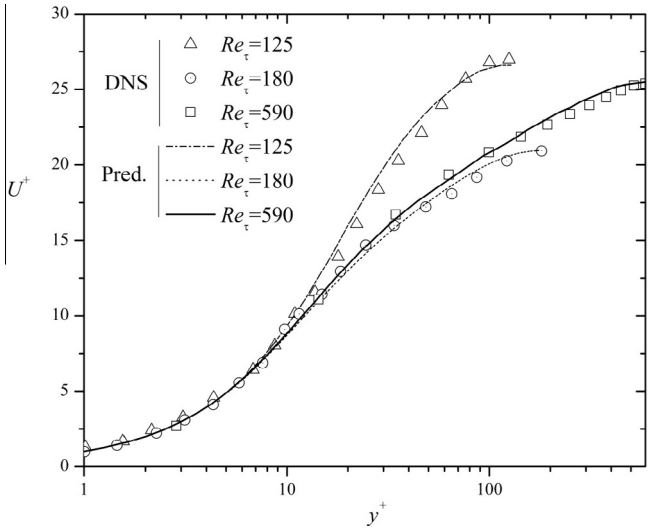

Fig. 21. Prediction of mean streamwise velocity profile for cases 8, 9, and 20. Flow and rheological parameters are described in Table 5.

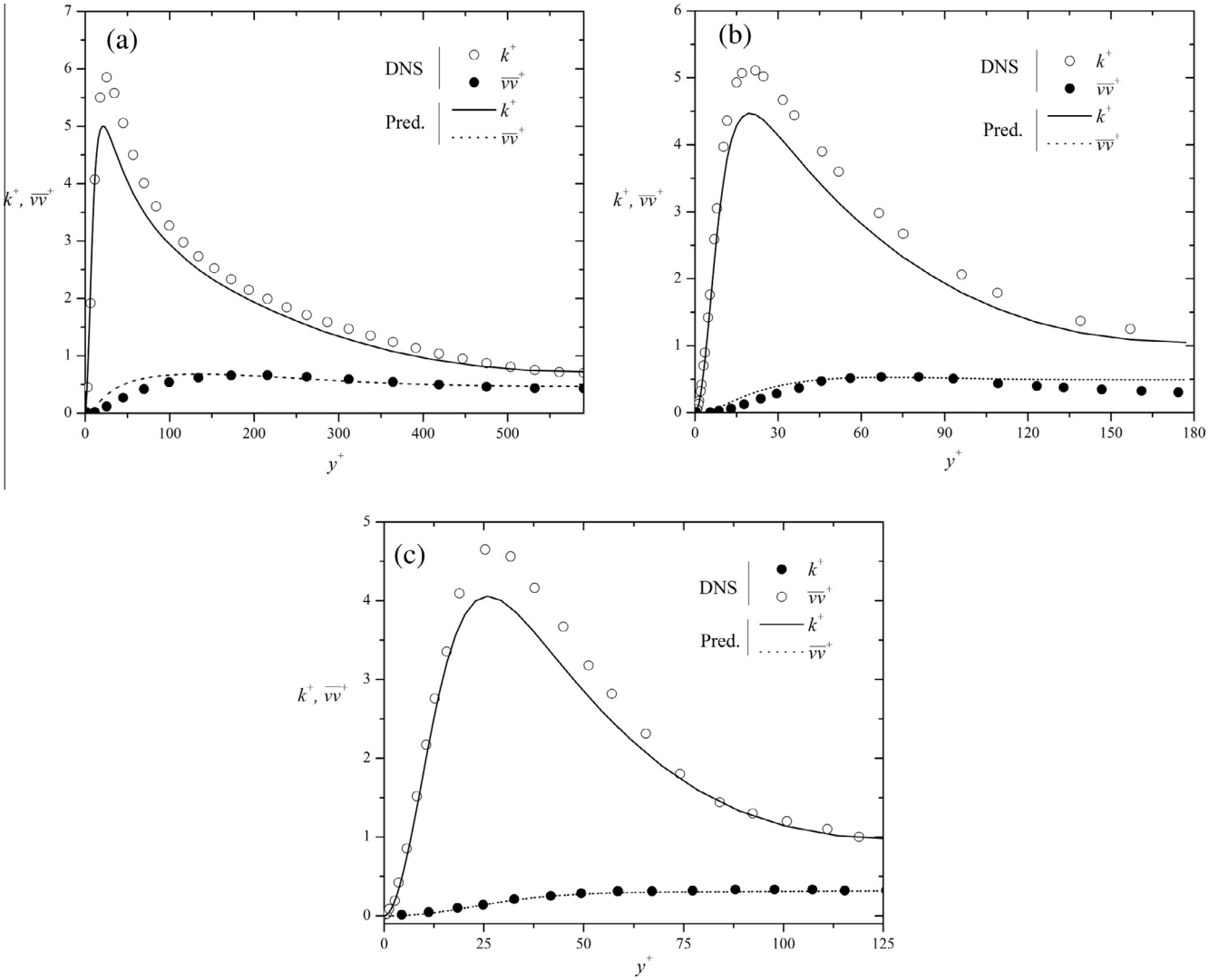

Fig. 22. Predictions of k^+ and $\overline{v^2}$ (a) case (20), (b) case (9), and (c) case (8). Flow and rheological parameters are described in Table 5.

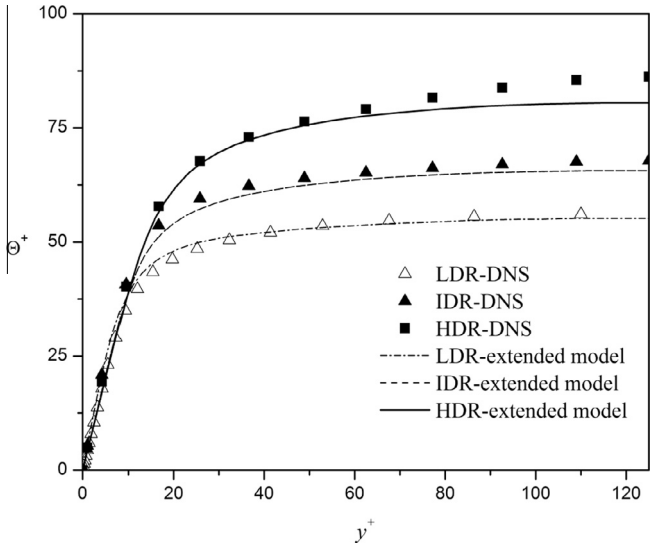

Fig. 23. Comparison between predicted and DNS data of mean temperature profile using extended closure of Kays [20] for cases, LDR (H4) IDR (H5), and HDR (H6). Flow and rheological parameters are described in Table 2.

6. Conclusions

In this work, the k–ε–$\bar{v}^2$–f model developed by Masoudian et al. [15], for turbulent flow of homogenous polymer solutions described by the FENE-P constitutive model, was improved. In addition, an appropriate closure was developed to compute the scalar Reynolds flux required by the thermal energy equation for the same fluids.

All previous attempts of RANS modeling of turbulent FENE-P fluid flows in a channel, which are valid up to the maximum drag reduction limit [15,19], contain two separate closures for the non-linear term (NLT_{ij}) in the conformation tensor evolution equation: one closure for the NLT_{kk} and another for NLT_{xy}. This feature, together with the reliance on the wall friction for some closures which was here removed, makes the model unattractive to be used in complex geometries. Instead, in this work a single Boussinesq-like relation is proposed for modeling the NLT_{ij} term, from which its trace can also be obtained thus making the model fully consistent.

Furthermore, since the closures are based on the *a priori* analysis of DNS data, a more extensive set of direct numerical simulations with different rheological parameters at different Reynolds

numbers was used to optimize the closures initially developed in [15]. As a consequence of this optimization process the closure for the wall normal polymer stress work was updated, which gives the current version of the model the capability of good prediction at very low Reynolds number flows. As referred above, the dependency of the previous model [15] on the wall friction velocity was removed to make the model more suitable to deal with complex geometries.

The performance of the proposed model is here assessed against 21 sets of DNS data for $Re_{\tau 0} = 128, 180, 300, 395, 590,$ and 1000 over a wide range of Weissenberg numbers for different values of L^2 as summarized in Table 5, thus confirming the robustness of the current model.

Regarding the Reynolds scalar fluxes, to the best of our knowledge this is the first ever closure used to deal with the heat transfer of viscoelastic fluids under turbulent flow conditions. The commonly used turbulent Prandtl number closure, originally developed by Kays [20] for Newtonian fluids, was extended to deal with viscoelastic turbulent flows after an extensive *a priori* analysis of DNS data. The model for the turbulent Prandtl number of FENE-P fluids was developed here for low drag reduction case at $Re_{\tau 0} = 180$, but its performance was assessed against sets of DNS data from low to high drag reduction and higher Prandtl numbers ($Pr = 5$), a value closer to that of polymer solutions. In this assessment, the Reynolds scalar flux model compared well with DNS.

Acknowledgements

The authors are grateful to FCT funding via project PTDC/EME-MFE/113589/2009. MM and FTP also wish to acknowledge funding FCT, FEDER, COMPETE, QREN and ON2 through project NORTE-07-0124-FEDER-000026-RL1-Energy. K. Kim gratefully acknowledges support from National Research Foundation of South Korea (NRF-2014K2A1A2048497).

References

[1] J.W. Hoyt, The effect of additives on fluid friction, ASME J. Basic Eng. 94 (1972) 258–285.
[2] J.L. Lumley, Drag reduction by additives, Annu. Rev. Fluid Mech. 1 (1969) 367–384.
[3] P.S. Virk, Drag reduction fundamentals, AIChE J. 21 (1975) 625–656.
[4] C.M. White, M.G. Mungal, Mechanics and prediction of turbulent drag reduction with polymer additives, Annu. Rev. Fluid Mech. 40 (2008) 235–256.
[5] I. Procaccia, V.S. L'vov, R. Benzi, Colloquium: theory of drag reduction by polymers in wall-bounded turbulence, Rev. Mod. Phys. 80 (1) (2008) 225.
[6] Y. Kawaguchi, T. Segawa, Z.P. Feng, P.W. Li, Experimental study on drag-reducing channel flow with surfactant additives spatial structure of turbulence investigated by PIV system, Int. J. Heat Fluid Flow 23 (5) (2002) 700–709.
[7] P.K. Ptasinski, B.J. Boersma, F.T.M. Nieuwstadt, M.A. Hulsen, B.H.A.A. Van den Brule, J.C.R. Hunt, Turbulent channel flow near maximum drag reduction: simulations, experiments and mechanisms, J. Fluid Mech. 490 (2003) 251–291.
[8] Y. Dubief, C.M. White, V.E. Terrapon, E.S.G. Shaqfeh, P. Moin, S.K. Lele, On the coherent drag-reducing and turbulence-enhancing behaviour of polymers in wall flows, J. Fluid Mech. 514 (2004) 271–280.
[9] C.D. Dimitropoulos, Y. Dubief, E.S.G. Shaqfeh, P. Moin, S.K. Lele, Direct numerical simulation of polymer-induced drag reduction in turbulent boundary layer flow, Phys. Fluids 17 (1) (2005) 011705.
[10] L. Thais, T.B. Gatski, G. Mompean, Analysis of polymer drag reduction mechanisms from energy budgets, Int. J. Heat Fluid Flow 43 (2013) 52–61.
[11] L. Thais, T.B. Gatski, G. Mompean, Some dynamical features of the turbulent flow of a viscoelastic fluid for reduced drag, J. Turbul. 13 (2012).
[12] C.F. Li, R. Sureshkumar, B. Khomami, Influence of rheological parameters on polymer induced turbulent drag reduction, J. Non-Newtonian Fluid Mech. 140 (1) (2006) 23–40.
[13] V.K. Gupta, R. Sureshkumar, B. Khomami, Passive scalar transport in polymer drag-reduced turbulent channel flow, AIChE J. 51 (2005) 1938–1950.
[14] B. Yu, Y. Kawaguchi, DNS of fully developed turbulent heat transfer of a viscoelastic drag-reducing flow, Int. J. Heat Mass Transfer 48 (21) (2005) 4569–4578.
[15] M. Masoudian, K. Kim, F.T. Pinho, R. Sureshkumar, A viscoelastic k–ε–v^2–f turbulent flow model valid up to the maximum drag reduction limit, J. Non-Newtonian Fluid Mech. 202 (2013) 99–111.
[16] F.T. Pinho, C.F. Li, B.A. Younis, R. Sureshkumar, A low Reynolds number turbulence closure for viscoelastic fluids, J. Non-Newtonian Fluid Mech. 154 (2) (2008) 89–108.
[17] P.R. Resende, K. Kim, B.A. Younis, R. Sureshkumar, F.T. Pinho, A FENE-P k–ε turbulence model for low and intermediate regimes of polymer-induced drag reduction, J. Non-Newtonian Fluid Mech. 166 (12) (2011) 639–660.
[18] T. Takahiro, Y. Kawaguchi, Proposal of damping function for low-Reynolds-number-model applicable in prediction of turbulent viscoelastic-fluid flow, J. Appl. Math. 2013 (2013).
[19] G. Iaccarino, E.S.G. Shaqfeh, Y. Dubief, Reynolds-averaged modeling of polymer drag reduction in turbulent flows, J. Non-Newtonian Fluid Mech. 165 (2010) 376–384.
[20] W. Kays, Turbulent Prandtl number – where are we, J. Heat Transfer Trans. ASME 116 (1994) 284–295.
[21] L. Thais, T.B. Gatski, G. Mompean, Temporal large eddy simulations of turbulent viscoelastic drag reduction flows, Phys. Fluids 22 (1) (2010) 013103.
[22] T. Ohta, M. Masahito, DNS and LES with an extended Smagorinsky model for wall turbulence in non-Newtonian viscous fluids, J. Non-Newtonian Fluid Mech. 206 (2014) 29–39.
[23] F.S. Lien, P.A. Durbin, Non-linear k–ε–v^2–f modeling with application to high-lift, in: Proceedings of the Summer Program 1996, Stanford University, 1996, pp. 5–22.
[24] P.A. Durbin, Near-wall turbulence closure modeling without damping functions, Theor. Comput. Fluid Dyn. 3 (1991) 1–13.
[25] W. Kays, M. Crawford, Convective Heat and Mass Transfer, McGraw-Hill, 1980.
[26] N. Kasagi, Y. Tomita, A. Kuroda, Direct numerical simulation of passive scalar field in a turbulent channel flow, ASME Trans. J. Heat Transfer 114 (1992) 598–606.
[27] M. Masoudian, K. Kim, F.T. Pinho, R. Sureshkumar, A Reynolds stress model for turbulent flow of homogeneous polymer solutions, Int. J. Heat Fluid Flow 54 (2015) 220–235.